# Visual Maladaptation in Contrast Domain

Dawid Pająk[a,b], Martin Čadík[b], Tunç O. Aydın[b], Karol Myszkowski[b], Hans-Peter Seidel[b]

[a]WPUT; [b]MPI Informatik

## ABSTRACT

In this work we simulate the effect of the human eye's maladaptation to visual perception over time through a supra–threshold contrast perception model that comprises adaptation mechanisms. Specifically, we attempt to visualize maladapted vision on a display device. Given the scene luminance, the model computes a measure of *perceived* multi–scale contrast by taking into account spatially and temporally varying contrast sensitivity in a maladapted state, which is then processed by the inverse model and mapped to a desired display's luminance assuming perfect adaptation. Our system simulates the effect of maladaptation locally, and models the shifting of peak spatial frequency sensitivity in maladapted vision in addition to the uniform decrease in contrast sensitivity among all frequencies. Through our GPU implementation we demonstrate the visibility loss of scene details due to maladaptation over time at an interactive speed.

**Keywords:** maladaptation, visual perception, contrast processing, human vision, temporal adaptation, high dynamic range

## 1. INTRODUCTION

It is consciously experienced by everyone that intense changes in illumination temporally cause a loss in visual sensitivity that is later recovered over a time period. In fact, considering the highly variant and temporally changing real world illumination, the human visual system (HVS) is virtually never fully adapted in practice. Due to this *maladaptation*, the visibility of some scene regions are reduced which would otherwise be perfectly visible if the HVS was fully adapted.

The temporal loss of visibility can often be tolerated in daily life, since a large fraction of sensitivity is recovered relatively fast in just a few seconds through neural mechanisms, and most real world objects are purposely designed to be strongly visible. However, some tasks require quick reaction times and undiverted attention. For those the rate of adaptation may not be sufficient. For instance, a car driver entering a forest highway after driving against the sun can be temporarily blinded for a short amount of time jeopardizing safety. In fact, computational methods have been proposed to determine the magnitude of vehicle display visibility under dynamic lighting conditions[1,2] enabling the validation of vehicle ergonomics and safety at design time. A more extreme case are fighter pilots who are exposed to much more drastic illumination changes, but regardless need to maintain near instant reaction capability at all times. On the other hand, the quickly recovered sensitivity may not be sufficient in environments containing low contrast objects. As an example, people often struggle to find their seats if they enter a movie theatre after the session started, while during the course of the movie the obstacles in the room become gradually visible due to the additional sensitivity recovery through the slower adaptation mechanisms based on chemical processes.

The aforementioned examples can benefit greatly from faithfully simulating the effect of maladaptation on visibility. Such a model should predict the visibility magnitude of both near– and supra–threshold scene details. Recent luminance based models[3–5] tend to explicitly focus on modeling maladaptation while ignoring other HVS aspects such as contrast sensitivity and visual masking. The modeling of the latter mechanism[6] requires a contrast based approach involving a transducer function. Current contrast domain frameworks, however, often do not account for luminance adaptation and contrast sensitivity, as well as the overall sensitivity loss and shift in peak sensitivity due to maladaptation.

Further author information: e-mail: {dpajak, mcadik, tunc, karol, hpseidel}@mpi-inf.mpg.de

[a] Westpomeranian University of Technology, Szczecin; [b] Max Planck Institut Informatik, Saarbrücken

An important consequence of maladaptation is the locality of resulting visibility loss in a scene. For instance, looking outside the window in a dark room on a sunny day, one will eventually adapt to the bright illumination outdoors and start seeing objects clearly. If at that instance the gaze is directed towards the interior, the observer will not be able to discriminate objects that are visually less apparent. Thus, at any given time details in some scene regions are less visible than others, as dictated by the current level of maladaptation. The problem is that it is often not possible to predict the direction the gaze will be shifted towards, and thus the illumination levels that will be observed in the next timestep. Similar to real–world scenes, the emerging HDR displaying technology coupled with the ever increasing size of display devices is also prone to such local losses of visibility. From an application perspective it is beneficial to simulate how the entire scene would look like under current adaptation conditions, which is not possible using current methods relying on a single adaptation level for the entire scene.

We present a system that renders a series of images of a scene as it would be seen by a maladapted eye over time. Each separate image corresponds to the visual perception of the scene at a time step while the sensitivity is recovered. The time course of adaptation is modeled by considering both neural mechanisms and pigment bleaching and regeneration. Our framework operates in contrast multi–scale domain and models supra–threshold effects like visual masking, while also accounting for contrast sensitivity and luminance (mal)adaptation usually considered only in luminance domain frameworks. We also model the shifting of peak frequency sensitivity in maladapted vision, which has not been considered by previous models. In the rest of the paper we first discuss related work (Section 2), followed by a new model for simulation of human maladaptation in contrast domain (Section 3). Next, we present, analyze and discuss the results of our system (Section 4) and finally we conclude and suggest ideas for future research (Section 5).

## 2. BACKGROUND

Previous models of time-course adaptation often operate on luminance and are not able to simulate visual phenomena locally. In this work, our goal is to simulate local maladaptation in *contrast domain* to account for supra–threshold mechanisms of vision as well as near–threshold. There were a few elaborate models of contrast perception proposed in history, but a vast majority of those were not concerned with the simulation of the time–course of maladaptation.

Ferwerda et al.[7] presented a computational model of visual adaptation. Their model captures the changes in threshold visibility, color appearance, visual acuity, and sensitivity over time using Ward's scaling tone mapping approach.[8] Ward's mapping is enriched by an offset parameter that is a function of time. The visual acuity is approximated by removing higher frequencies according to Schaler's measurements. This is a simplistic approach because human sensitivity to contrast also decreases for lower frequencies. A photoreceptor-based global time–dependent tone mapping method presented by Pattanaik et al.[4] is built on parts of an advanced Hunt's model of color vision.[9] By means of the adaptation model the method accounts for time dependency of retinal adaptation mechanisms for both cones and rods. However, as this adaptation model and the method itself are global they can simulate neither local adaptation mechanisms nor human contrast sensitivity. Irawan et al.[5] devised a model of low vision that is able to simulate the performance of an impaired or aged human visual system. The model is based on the combination of histogram adjustment[10] and Pattanaik et al.'s[4] global tone mapping methods. Due to the maladapted threshold-versus-intensity function (*tvia*), it can mimic the viewer's changing adaptation. The method is able to simulate the effect of maladaptation, but only at the threshold level and only globally for the whole image. However we are also interested in the supra–threshold effects of maladaptation in addition to visual perception around the threshold level.

Pattanaik et al.[3] proposed an advanced multiscale model of adaptation and spatial vision. As the model is based on spatial decomposition it can predict spatial contrast sensitivity behavior. The authors proposed gain functions that should be valid both for near– and supra–threshold luminance levels. However, the model does not comprise the time course of adaptation and is therefore unable to simulate effects of maladaptation. More recently, Mantiuk et al.[11] proposed a multiscale framework for perceptual processing of contrast. The method simulates supra–threshold perception (compression) of contrasts on multiple scales using transducer functions. However, contrasts still need to be compressed in a response space and yet another and more artificial compression is accomplished by the optimizer due to its weighting coefficients. The output of the optimization

problem solver is therefore hard to calibrate for the correct reproduction of luminance perception. Moreover, the method in fact does not simulate human adaptation.

HVS models involving maladaptation have been also been proposed in the context of detecting the visibility loss on display devices due to dynamically changing illumination.[12] While in this work temporal maladaptation is modeled in the contrast domain, they consider global adaptation and only output a "visibility map" that depicts distortions in the image structure similar to image quality assessment metrics, instead of rendering images of the scene appearance in a maladapted state. Furthermore, they don't model the change in spatial frequency sensitivity due to maladaptation, which we discuss in detail in Section 3.2.

## 2.1 Human Contrast Sensitivity in Maladapted State

Vision literature concerning the modeling human spatial *contrast sensitivity in an adapted state* usually through a *contrast sensitivity function* (CSF) is rich.[13] Much work has also been done on *temporal contrast sensitivity*,[14] i.e. the sensitivity of HVS to the spatial frequencies over time, as this (and so called critical flicker frequency) was crucial in the design of first CRT display devices. However, measurements of CSF in maladapted states are hardly that obvious, perhaps due to the complicated testing and evaluation process. Maladapted luminance intensity thresholds are measured only for simple stimuli without any variation of spatial frequency.[15] Consequently, in the rest of this section we discuss findings on the shape of CSF in maladapted conditions.

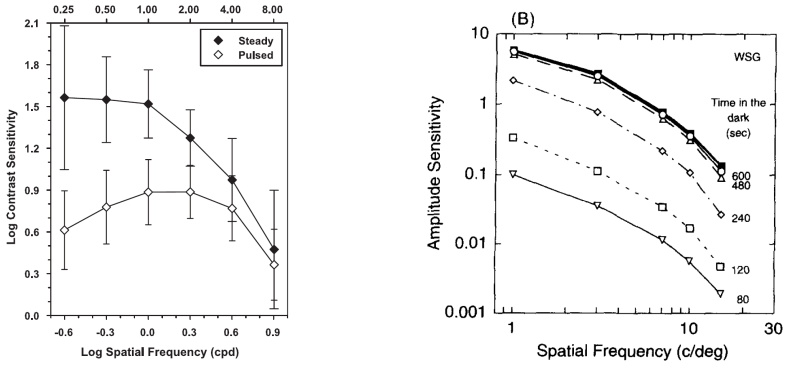


Figure 1. Measurements of maladapted contrast sensitivity. Left: the shape of CSF for steady (adapted) state and for briefly pulsed (maladapted) stimulus, adapted from[16], right: amplitude sensitivity functions during dark adaptation, adapted from [17] (the right image shows the amplitude sensitivity functions (ASF); one can obtain CSF from ASF by multiplying with the background luminance).

The encoding of contrast within the human visual system is thought to be mediated by two processing streams: the magnocellular (M) and parvocellular (P) pathways.[18] To investigate the effect of the pathways, Lenova et al.[19] and Alexander et al.[16] measured contrast sensitivity using two different paradigms. In the steady–pedestal paradigm, they briefly presented a test stimulus against a continuously presented adaptation field. In the pulsed–pedestal paradigm, the test stimulus was presented simultaneously with the adapting field. The steady–pedestal paradigm favors the M pathway, while the pulsed–pedestal paradigm favors the P pathway. The measured mean contrast sensitivity function for control subjects for steady–pedestal has a low–pass shape, while for the pulsed–pedestal it has a band–pass shape, see Fig. 1 (left).

On the other hand, Hahn et al.[17] found the CSF to be invariant in shape during dark adaptation. Differently from Leonova et al.[19] who presented stimuli only briefly to observers during experimentation, Hahn et al. measured a longer time course of dark adaptation ranging from seconds to hundreds of seconds, see Fig. 1 (right). This suggests that the transition from original to destination stimuli is very fast in terms of sensitivity to spatial frequencies (as modulated by P pathway), but much slower in terms of overall sensitivity to contrast. In other words, the shift in frequency sensitivity happens almost instantly and is retained during the time course of adaptation to the destination stimulus.

In our method, we use Daly's CSF[20,21] and we were tempted to simulate the aforementioned transition behavior by using current adaptation luminance as input parameter $L_a$ of the maladapted observer. This

approach, combined with the use of *maladaptation ratio* resulted in reasonable time course shape of the CSF. (The maladaptation ratio is approximated as $cvi(L_b)/cvia(L_b, L_a)$, where $cvi$ and $cvia$ are the contrast versus intensity functions for adapted and maladapted eye, respectively, $L_a$ is the current adaptation luminance, and $L_b$ is the current background luminance[12]). However, this method implies the assumption that the spatial frequency sensitivity characteristics of the HVS remains constant in maladapted states, since the CSF we use was measured for the adapted eye. We can neither calibrate nor justify this approach as we were not able to find a sufficient amount of maladapted CSF experimental measurement data.

Therefore, in our model we incorporate the shift in frequency sensitivity due to maladaptation to the maladaptation ratio approach. Following an abrupt illumination change, we instantly modify the shape of the CSF to reflect the spatial frequency sensitivity in the target state, and then increase the sensitivities globally using the maladaptation ratio over the time course of adaptation. Our method is supported by experimental evidence: the sensitivity after sudden illumination change drops down drastically and when it is (at least partially) regenerated the curve already has the invariant shape of the target (compare Fig. 1 right with Fig. 5 right).

## 3. SIMULATION OF VISUAL MALADAPTATION

The data flow of the proposed model for human contrast perception in maladapted states is illustrated in Fig. 2 for the steady–state. We assume that the input HDR image is calibrated in cd/m$^2$ units. First, we construct background luminance and local adaptation maps $(L_b, L_a)$, which are used both for contrast processing and final display purposes. The adaptation map is modified over time to model the temporal adaptation. Simultaneously, we decompose the input image into the contrast representation ($C$) using the Laplacian pyramid.[22] We then process physical contrast by a model of *maladapted scene observer* depending on sensitivity to spatial frequencies as well as on the current adaptation state to get the perceptual contrast responses ($R$). The response values are transformed by inverse *adapted display observer* model to obtain physical display contrast. All contrast processing steps are performed on multiple scales simultaneously. Consecutively, the physical contrast is converted to display luminance map ($L_d$) and colors are processed ($I_{\text{corr}}$). Finally, the inverse display model produces the output code values ($I_{\text{out}}$) that are shown on the display device.

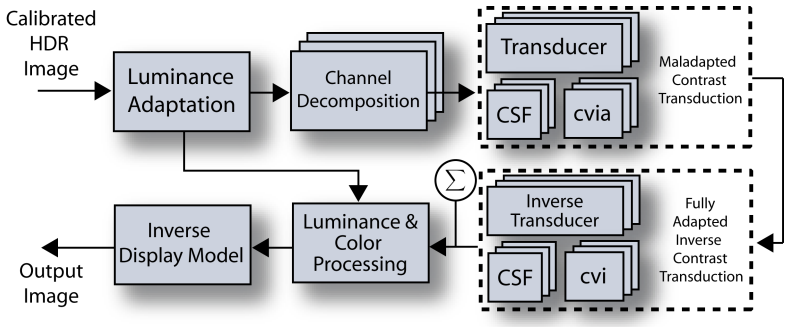


Figure 2. Flow chart of the proposed method. See text for details.

### 3.1 Adaptation Map

The adaptation map $L_a$ represents the actual state of local adaptation of the observer. The construction of the *local adaptation* map is based on the actual *background luminance map* $L_b$ and on the previous course of local adaptation (see Section 3.4 for the details on temporal adaptation). Background luminance $L_b$ is the actual stimulus of an observer and is calculated for each input frame as the blurred image of input luminance (as the contrast sensitivity function was measured for foveated vision we blur the luminance conformably to one visual degree $(1^\circ)$[10]). To accomplish this we use the Gaussian filter with the kernel size $K = \frac{2d}{p}\tan(\frac{\pi}{360})$, where $p$ is the pixel size (in meters) and $d$ is the observer's distance from the display (in meters).

Similarly to Irawan et al.[5] we model the adaptation due to human rods and cones separately. To obtain a single response value, Hunt [9, Sec. 31.8.2] proposed to sum the achromatic cone and rod responses up. The

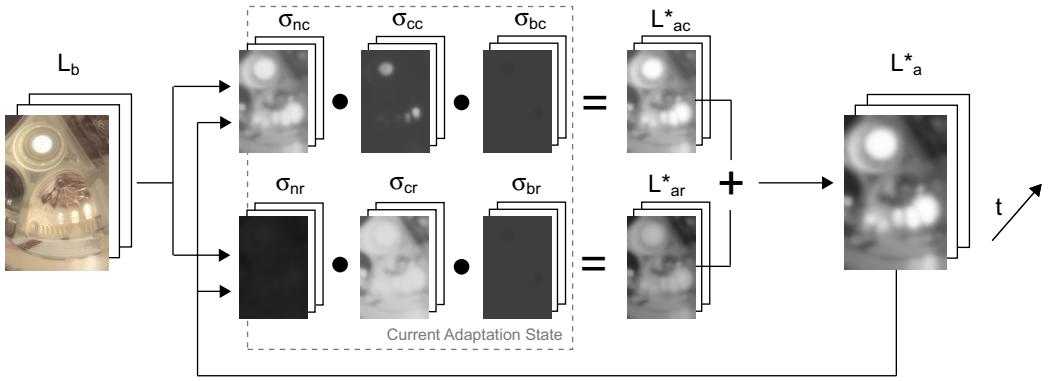


Figure 3. Visual illustration of the local adaptation processing. Temporal behavior is modeled for rod $L^*_{ar}$ and cone $L^*_{ac}$ adaptations separately, which are computed from adaptation maps $(\sigma_{bc}, \sigma_{cc}, \sigma_{nc}, \sigma_{br}, \sigma_{cr}, \sigma_{nr})$ that model various adaptation mechanisms. These adaptation maps are updated at each timestep using the current background luminance map $L_b$. In maladaptation computation (see Sec. 3.2), a compound adaptation map $L^*_a$ is obtained by adding adaptation maps for rods and cones. HDR image courtesy of Paul Debevec.

current adaptation luminance $L^*_a$ is therefore obtained (as also illustrated in Fig. 3) as a sum of cone $(L^*_{ac})$ and rod $(L^*_{ar})$ adaptations: $L^*_a = L^*_{ac} + L^*_{ar}$, where $L^*_{ac} = \sigma_{bc} \cdot \sigma_{cc} \cdot \sigma_{nc}$ and $L^*_{ar} = \sigma_{br} \cdot \sigma_{cr} \cdot \sigma_{nr}$. Factor $\sigma_b$ accounts for the *photopigment bleaching and regeneration*: $\sigma_b(L_b) = 1/p(L_b)$, where $p(L) = I_0/(I_0 + L)$ and $I_0 = 10^4$ cd/m$^2$. To model *neural adaptation mechanisms*, we calculate $\sigma_n$ (fast neural adaptation) and $\sigma_c$ (slow neural adaptation) for rods and cones using the equations proposed by Irawan et al.[5] Note however that our implementation of human adaptation is local (i.e., we have the adaptation map) and all of the factors mentioned above $(L^*_{ac}, \sigma_{bc}, \sigma_{cc}, \sigma_{nc}, L^*_{ar}, \sigma_{br}, \sigma_{cr}, \sigma_{nr})$ are not single values, but complete maps spanning the whole image.

For the subsequent processing (CSF filtering, *cvi*, *cvia* functions), we need to convert the adaptation values $L^*_{\cdot}$ scaled in hypothetical *perceptual adaptation* units back into the physical units. In other words, we are searching for an adaptation map $L_a$ in physical luminance units that would evoke the actual maladapted state $L^*_a$ in the observer's visual system. To do this, we numerically invert the function $L^*_a$ and set $L_a = L^{*-1}_a(L^*_a(L^*_{ac}, L^*_{ar}))$. Note that for the fully adapted observer this results in $L_a = L_b$ as expected, but for the maladapted observer, the behavior of this function is more complex (see Section 3.4).

Figure 4. Comparison of the effect of global and local adaptation. Left: global adaptation (using global values $L_{ag}$ and $L_{bg}$), right: local adaptation (using local $L_b$ and global $L_{ag}$). Notice that local background luminance map allows to simulate different sensitivity to spatial contrasts according to varying illumination in the scene.

For experimental visual analysis and illustration purposes we allow the use of the *global adaptation* value $L_{ag}$ instead of the local adaptation map. We can calculate the global background luminance $L_{bg}$ as a geometric mean of the input luminance $L$ for each pixel: $L_{bg} = (\Pi^n L)^{1/n}$ and similarly we obtain the global adaptation

luminance $L_{ag}$. Global $L_{ag}$ is useful for the analysis of static images, where it would be hard to change local adaptation map $L_a$ manually if a refence HDR image depicting the adaptation state is not present. Note that in the rest of the figures the background luminance ($L_b$) is still local even in global adaptation ($L_{ag}$) case (see Fig. 4-right), with the exception of Fig. 4-left where we illustrate global adaptation $L_{ag}$ with global background $L_{bg}$ luminance for comparison.

### 3.2 Maladapted Spatial Sensitivity to Contrast

To account for sensitivity to spatial frequencies, we utilize the contrast sensitivity function (CSF) proposed by Daly.[20,21] The corresponding spatial frequency $\rho$ (in c/deg) for each level $l$ (starting from 1) of Laplacian pyramid is obtained as $\rho = K/2^{(l-1)}$. The size of the image (in $X \times Y$ pixels) in visual degrees is $i^2 = \max(X, Y)/K$. Given spatial frequency $\rho$ in $c/deg$, observer distance $d$ in meters, image size $i^2$ in visual degrees, and current background luminance level $L_b$ (in cd/m$^2$), and neglecting orientation and eccentricity we can calculate the sensitivity $S_a$ for contrast magnitudes $C$ (in Weber's units) for each pixel at each level $l$ of pyramid:

$$S_{al} = CSF(\rho, \theta, L_{bl}, i^2, d, C_l), \tag{1}$$

where the coarser background luminance map $L_{b(l+1)}$ is a downsampled from the finer scale map $L_{bl}$. We account for maladaptation by computing the maladaptation fraction as given in:[12]

$$S_{ml} = S_{al} \cdot \frac{cvi(L_{bl})}{cvia(L_{bl}, L_{al})}, \tag{2}$$

where $S_{ml}$ is the sensitivity in the maladapted state, $S_{al}$ is the sensitivity at the fully adapted state, $L_{bl}$ is the current background luminance and $L_{al}$ is the current adaptation luminance. The subscript $l$ indicates the scale of each map.

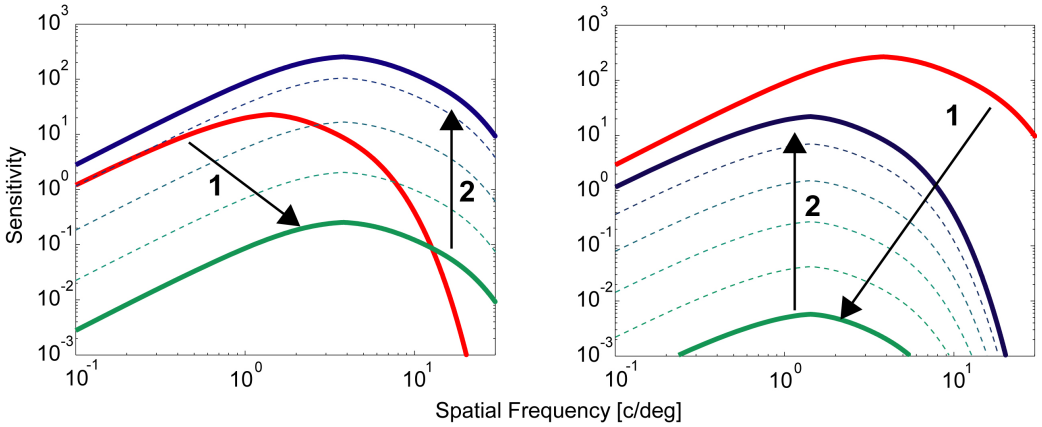


Figure 5. Simulation of time-course of contrast sensitivity for a maladapted observer. Left: transition from dark to bright, Right: transition from bright to dark environments (dark adaptation).

Fig. 5 shows the change in shape of CSF between two adapted states. In the left image, a subject is adapted to a dark environment. Accordingly, her sensitivity to contrast is low and shifted to low spatial frequencies (blue curve). After the exposition to a bright environment, the sensitivity rapidly shifts towards higher frequencies (arrow 1), but due to the maladaptation (as one is blinded by strong light for some time) the sensitivity is still very low (green curve). However, sensitivity is restored over time (arrow 2) to reach the final fully adapted state for the bright environment (red curve). The process is similar for a subject adapted to the bright environment (red curve in Fig.5 right). First, the sensitivity drops rapidly (arrow 1), shifts to the low frequencies (green curve) and consecutively it regenerates (arrow 2) to the final dark–adapted state (blue curve). The described behavior is in accord with psychophysical experiments conducted by Hahn and Geisler [17, Fig. 5, 6], who measured that the CSFs are nearly identical throughout the course of dark adaptation. Naturally, the two processes differ in the speed of the sensitivity regeneration and we describe our implementation of the temporal aspects of adaptation below.

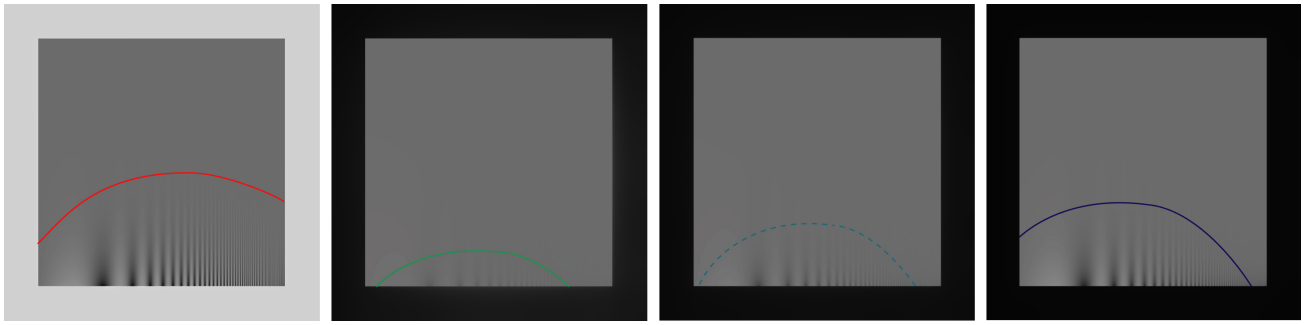

Figure 6. Classical Campbell-Robson contrast sensitivity chart for dark adaptation. From left to right: (1) fully adapted state in a relatively bright environment (adaptation luminance 112 $cd/m^2$), (2) background luminance was decreased to 2 $cd/m^2$, the contrast sensitivity moves to lower frequencies, but due to maladaptation, it is basically very low, (3) sensitivity regenerates according to dark adaptation time-course, (4) final fully adapted state (adaptation luminance 3 $cd/m^2$). The curves show the thresholds observed from approximately 30 centimeters at original paper size.

### 3.3 Contrast Transduction

The visual sensitivity to a contrast patch of a certain spatial frequency decreases with the presence of other similar frequency contrast. Daly's Visible Differences Predictor (VDP)[20] accounts for this effect known as *visual masking* using a threshold elevation map. This approach trades off supra–threshold contrast interval for near–threshold precision. Such a trade–off is not suitable to our purposes, as real–world scenes are expected to comprise contrast well above the visibility threshold. Thus, in our model we employ the *transducer* function $T$ described in[23] based on the premise that it is tuned for both near–and supra threshold precision. The contrast $C$ at each scale is processed separately as follows:

$$R_{al|ml} = T(C, S_{al|ml}) = \frac{3.291 \cdot [(1 + (S_{al|ml}C)^3)^{1/3} - 1]}{0.2599 \cdot (3.433 + S_{al|ml}C)^{0.8}}, \tag{3}$$

where $R_{al|ml}$ is adapted or maladapted human perceptual response to contrast, $S_{al|ml}$ is the sensitivity at either maladapted or fully adapted state. The constants are taken from Wilson's work without any change. The monotonically increasing behaviour of the transducer function enables a fast inversion through the use of a lookup table stored in GPU memory.

### 3.4 Temporal Adaptation

Temporal adaptation can be modeled through two separate exponential decay functions; one for *pigment bleaching and regeneration* and another for *neural adaptation*.[5] For simplicity, we describe the adaptation process generically, but recall (Sec. 3.1) that the final adaptation map $L_a^*$ is combined from six values that possess different time constants.

The time course of the neural adaptation mechanism from perceived luminance $L_0^*$ at time $t = 0$, to $L_\cdot^*$ (where $L_\cdot^*$ is $\sigma_{cc}, \sigma_{nc}, \sigma_{cr}, \sigma_{nr}$) is modeled as follows:

$$L_\cdot^* = L_b^* + (L_0^* - L_b^*)\, e^{\frac{-t}{t_0}}. \tag{4}$$

The contribution of neural adaptation to temporal recovery of visual sensitivity is modeled by updating the *cvia* function at each time step using the current $L_a^*$. We set $t_0$ to 0.08 seconds for cones, and 0.15 seconds for the rods.[5]

Pigment bleaching and regeneration (modeled by $\sigma_{bc}$ and $\sigma_{br}$), unlike neural adaptation, are slow and not symmetric for dark and bright adaptation. Assuming that the amount of signal transmitted by receptors is proportional to $p \cdot L$, the fraction of unbleached pigments $p$ is computed as in Equation 5:

$$p = p(L_b) + (p_0 - p(L_b))\, e^{\frac{-t}{t_0 \cdot p(L_b)}}. \tag{5}$$

In the steady state, $p(L)$ is $I_0/(I_0 + L)$ where $I_0$ is $10^4$ $cd/m^2$. The time constant $t_0$ is set to 110 and 400 seconds for cones and rods, respectively.

### 3.5 Luminance and Color Processing

The inverse transducer converts maladapted contrast responses $R_m$ to the luminance values $L_m$. By summing all the levels of the Laplacian pyramid we obtain the maladapted luminance map. This map represents the hypothetical output of the display device that would evoke the same perception of *contrast* in a fully-adapted display observer as the original HDR scene in the maladapted observer. However, to account also for the luminance sensitivity, we transform $L_m$ using the S–shaped function as follows:

$$L_d = \frac{L_m}{L_m + \bar{L_a^*}}; \qquad \bar{L_a^*} = (\Pi^n L_a^*)^{1/n}, \tag{6}$$

where $L_d$ is the output display luminance, $L_m$ is the luminance value we obtained from of inverse observer model, and $\bar{L_a^*}$ is a geometric average of the current adaptation luminance map. Note that the value of $L_a^*$ accounts for the current (mal)adaptation state and therefore the S–shaped function results in dark images for dark adaptation scenario and bright images for adaptation to bright scenes, and the sensation will improve according to the temporal adaptation as described above.

As our aim is the simulation of maladaptation in contrast domain (and not the simulation of color vision phenomena), we perform only very simplified color processing. Simply put, all the above described processing happens on achromatic channel only. However, as the local adaptation map $L_a$ is calculated as a combination of the human rod and cone responses ($L_{ar}, L_{ac}$, refer to Section 3.4) we can utilize them for color processing. In the absence of a model of color perception specialized in maladapted HVS states, we desaturate the colors as follows: $I_{\text{corr}} = I^s$ (for each color channel $I$ separately) using the following saturation coefficient $s = L_{ac}/(L_{ac} + L_{ar})$, where $L_{ac}$ and $L_{ar}$ are current cone and rod adaptation map values, respectively.

### 3.6 Inverse Display Model

Our simple display model consists of three parameters, the maximum and minimum display luminance, and a gamma value which we set to 1/2.2. The gamma corrected values $I_{\text{corr}}$ are fitted to the luminance range of the display by a simple linear mapping. Our interface allows the user to control the display luminance range, this way a variety of display types can be approximated. For a more precise simulation of specific displays the linear mapping can be replaced by the display response function.

## 4. RESULTS

In this section we discuss our results, implementation details, and the other possible uses of the model. Please refer to supplemental materials (`http://mpi-inf.mpg.de/~mcadik/maladaptation`) for further results.

A visual verification of maladapted contrast sensitivity behavior (described in Sec. 3.2) is presented in Fig. 6. We augmented the Campbell-Robson chart with a frame of uniform luminance and generated two different HDR images (an initial and a final) to simulate the dark adaptation. The results show both the shift in peak frequency and the drop and regeneration of absolute sensitivity as expected. As we want to illustrate only the contrast processing in this figure, we simplify the equation (6) to $L_d = L_m/(L_m + k)$, where $k$ is set to 100 $cd/m^2$. Otherwise the maladapted images (the two middle images in Fig. 6) would be too dark to visualize. Compare the output of our model in Fig. 6 with Fig. 5 and 1 (right).

In Fig. 7 we compare our results to the approach of Irawan et al.[5] The reference method (upper row) is based on global tone mapping function and global background luminance ($L_{bg}$), while our approach (bottom row) operates on contrasts and utilizes local background luminance ($L_b$). In both cases global adaptation luminance $L_{ag}$ is assumed. Therefore our method accounts for diverse perception of bright and dark areas of the scene. One can notice a difference in the fully adapted state as well (Fig. 7-rightmost images): in our model, the stained glass window is reproduced sharply and all the details are visible, while the dark area below the desk is blurred, which is the expected behavior. Note that by considering local background luminance ($L_b$) we ignore changes in the state of adaptation due to attending different image regions as a consequence of the saccadic eye motion. We rather visualize the image appearance under the condition that the eye attends locally each respective region without any gaze change. Thus, Fig. 7 (bottom row) presents a synthetic summary how each specific region will be seen under this assumption, but the overall image appearance may not be presented precisely. Irawan

Figure 7. Comparison of our method to the approach of Irawan et al.[5] simulating the fast adaptation from a dark environment ($10^{-4}$ cd/m$^2$) to the stained glass (17 cd/m$^2$). Top row: method of Irawan et al. can not simulate differences in perception of contrasts in bright and dark parts of the scene, however our method can (bottom row). Columns from left to right: $t = 0.01$s, $t = 0.02$s, $t = 0.05$s, $t = 0.1$s, $t = 60$s (fully adapted state). HDR image courtesy of OpenEXR.

used another extreme approach by considering global background $L_{bg}$ (Fig. 7 – upper row), in which case it is implicitly assumed that through the gaze direction changes the eye adaptation tends to some average luminance in the scene. Since the most dramatic changes in light adaptation take place during the time required just for a couple of fixations this assumption is also not realistic in particular for video, while it is commonly used. Thus, Fig. 7 (upper row) gives perhaps a better prediction of overall image impression (except that no frequency processing is accomplished), but the local detail visibility might be better predicted in Fig. 7 (bottom row).

In Fig. 8 we illustrate an application of our approach to analysis of the visibility of a display and controls on the panel in a flight control room. Left column shows fully adapted state, where all the details are well visible. After the adaptation to the bright sky however, those details are not noticeable for some seconds.

Our system enables also to simulate even more complex scenario (see Fig. 9) where in lack of opposing evidence we consider local adaptation $L_a$ and background $L_b$ maps, in which case each local region in the image

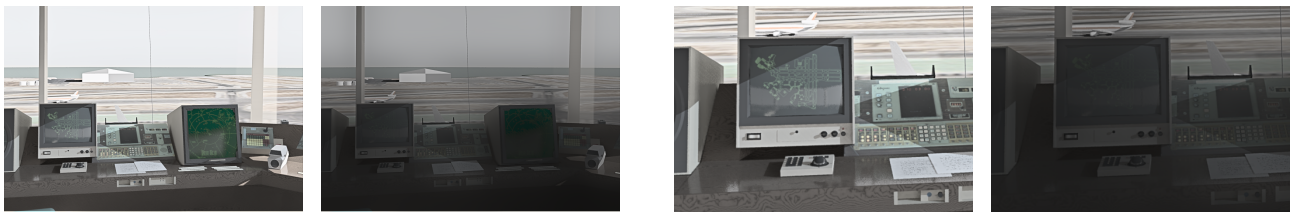

Figure 8. Rendering of the interior of an airport control tower. Left: fully adapted state (178 cd/m$^2$). Right: maladaptation due to a previous exposition to the bright sky ($10^4$ cd/m$^2$), $t = 0.5$s. Compare the visibility of displays and controls in close-ups (right pair). HDR image courtesy of Greg Ward.

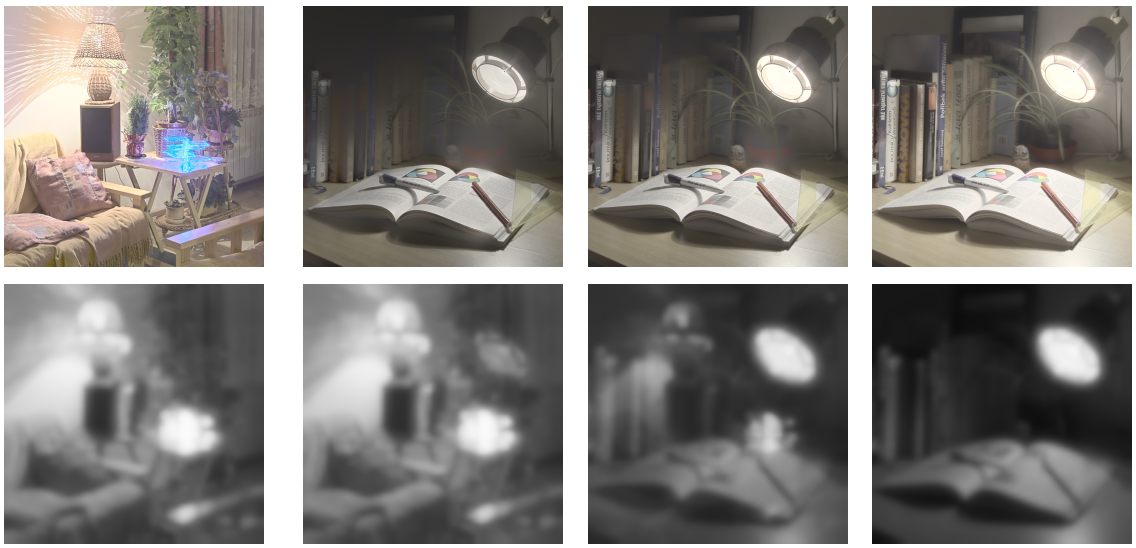

Figure 9. Simulation of maladaptation in a complex hypothetical scenario. Top row, from left to right: (1) fully adapted state in a relatively bright living room (adaptation luminance 70 $cd/m^2$), (2) rapid movement to a work-room (8 $cd/m^2$), time $t = 0.02$s, (3) sensitivity regenerates and aftereffects diminish ($t = 0.1$s), (4) in $t = 0.5$s the observer reached nearly fully–adapted state, but some dark details are washed out, due to the dim illumination of the work–room. Bottom row: states of adaptation maps $L_a$ corresponding to the upper images. As the values in adaptation maps are HDR, they were tone mapped using the global version of Reinhard's[24] TMO for the display purpose.

has also corresponding local adaptation. Imagine an observer who is adapted to relatively bright illumination of a living room and then she instantly moves to her desk in a dim work–room. For a moment, while her sight is being regenerated, she does not see the details in some parts of the scene due to the previous adaptation to much brighter environment. The vision reaches the fully adapted state in some seconds, but due to the low illumination of the work-room, the vision is still not sharp in dark parts of the scene.

### 4.1 Fast GPU Implementation

In order to get real–time performance, we moved perceptual (contrast transduction, calculation of maladaptation, local cones and rods adaptation) and image processing (laplacian pyramid, tone-mapping) parts of the algorithm to the GPU. For the purpose of real–time HDR movie processing we also had the radiance format decompression realized on the GPU. Because of that, we are able to achieve interactive frame rates on mainstream hardware. Our test system is based on Intel Core2 3.0Ghz CPU, 4GB of RAM and NVidia GTX260 GPU. The average performance is around 75 fps for 1024x1024 HDR image. After processing the data we manually copy the resulting texture to GUI surface. Displaying the image directly would improve the speed even further.

### 4.2 Simulating Maladaptation in LDR Images

Another possible application of our model is the simulation of maladaptation effects on contrast perception in an ordinary (LDR) image, see Fig. 10. Let us assume that only an LDR image is available, but we want to know how its appearance will be affected due to the maladaptation. It is possible to perform inverse tone mapping[25] and derive a reasonable approximation of adaptation map. Having a scene referred HDR image as the adaptation pattern, we can simulate appropriate HVS reaction for arbitrary LDR image as follows: we run the model for the HDR image and we keep the contrast responses $R_a$ for fully adapted observer and for a particular maladapted state $R_m$, then we linearize the LDR image using inverse gamma correction and decompose it using Laplacian pyramid. To simulate maladaptation in the LDR image, we multiply the values in the Laplacian pyramid as

follows:

$$C'_{i,j,l} = C_{i,j,l} \cdot \frac{R^m_{i,j,l}}{R^a_{i,j,l}}, \tag{7}$$

where $C$ is the current LDR contrast value for pixel $i, j$ and level $l$ of Laplacian pyramid. The final LDR image with the simulated maladaptation effect is obtained by adding $C'$ at all the levels of modified Laplacian pyramid. In this special case we simulate only the effect of maladaptation to the perception of contrasts, as we omit the luminance processing (i.e. we do not involve equation (6)).

Figure 10. Simulation of maladaptation in two different LDR images. In each pair: left: original LDR image. Right: maladaptation simulation using the background luminance from the HDR image (200cd/m$^2$) obtained by the inverse tone mapping. Simulated adaptation luminance: 20cd/m$^2$. HDR image courtesy of Allan Rempel et al.[25]

## 5. CONCLUSION

We presented an efficient, real–time visual maladaptation framework capable of rendering images of a scene as perceived by a maladapted observer. Our model operates on contrast domain and accounts for supra–threshold HVS mechanisms such as visual masking, as well as luminance adaptation and contrast sensitivity as a function of spatial frequencies that have often been neglected by previous contrast domain methods. We also model the shift in spatial frequency sensitivity due to maladaptation, which we found to have a significant effect on scene visibility. We discuss a fast GPU implementation that enables interactive rendering of maladapted images. Our system can potentially be used to simulate human vision in illumination conditions causing extreme maladaptation in real–world scenarios such as driving.

### 5.1 Limitations and Future Work

As the model is not targeted for the simulation of HVS *color processing*, it mainly operates on the achromatic channel only. Therefore it does not account for chromatic adaptation, color aftereffects and other phenomena of color vision; but we believe those can be pertinently included, if necessary.

The model assumes to input a calibrated HDR image and by modeling of the HVS features it is accordingly able to perform the *HDR tone mapping* task (for a calibrated HDR image). However, as the primary goal of the model is the correct simulation of the HVS contrast processing, the results for some extremely high dynamic range or not calibrated images can not outperform the results of specifically tuned tone mapping operators. Note however, that the HVS is also unable to see all the details in the scene simultaneously for extremely high dynamic ranges. From this point of view, the results of many "successful" tone mapping operators are not perceptually correct, as indicated by recent experimental studies.[26,27]

## REFERENCES


[1] Krantz, J. H., Silverstein, L. D., and Yeh, Y.-Y., "Visibility of transmissive liquid crystal displays under dynamic lighting conditions," *Hum. Factors* **34**(5), 615–632 (1992).

[2] Silverstein, L., "Display visibility in dynamic lighting environments: Impact on the design of portable and vehicular displays," (2003). IDMC'03, Taipei, Taiwan.

[3] Pattanaik, S. N., Ferwerda, J. A., Fairchild, M. D., and Greenberg, D. P., "A multiscale model of adaptation and spatial vision for realistic image display," in [*SIGGRAPH '98*], 287–298, ACM Press (1998).

[4] Pattanaik, S. N., Tumblin, J., Yee, H., and Greenberg, D. P., "Time-dependent visual adaptation for fast realistic image display," in [*SIGGRAPH '00*], 47–54 (2000).

[5] Irawan, P., Ferwerda, J. A., and Marschner, S. R., "Perceptually based tone mapping of high dynamic range image streams," in [*EGSR'05*], 231–242 (2005).

[6] Ferwerda, J. A., Pattanaik, S. N., Shirley, P. S., and Greenberg, D. P., "A model of visual masking for computer graphics," in [*SIGGRAPH'97*], 143–152 (Aug. 1997).

[7] Ferwerda, J. A., Pattanaik, S. N., Shirley, P., and Greenberg, D. P., "A model of visual adaptation for realistic image synthesis," in [*SIGGRAPH '96*], 249–258, ACM, New York, NY, USA (1996).

[8] Ward, G., "A contrast-based scalefactor for luminance display," *Graphics Gems IV* , 415– 421 (1994).

[9] Hunt, R. W. G., [*The reproduction of colour*], Fountain Press, 5. ed. ed. (1995).

[10] Larson, G. W., Rushmeier, H., and Piatko, C., "A visibility matching tone reproduction operator for high dynamic range scenes," *IEEE TVCG* **3**, 291–306 (1997).

[11] Mantiuk, R., Myszkowski, K., and Seidel, H.-P., "A perceptual framework for contrast processing of high dynamic range images," in [*APGV '05*], 87–94, ACM Press (2005).

[12] Aydın, T. O., Mantiuk, R., and Seidel, H.-P., "Predicting display visibility under dynamically changing lighting conditions," *EUROGRAPHICS* **28**(3) (2009).

[13] Barten, P. G., [*Contrast sensitivity of the human eye and its effects on image quality*], SPIE (1999).

[14] Kelly, D. H., "Spatio-temporal frequency characteristics of color-vision mechanisms," *Journal of the Optical Society of America (1917-1983)* **64**, 983–+ (July 1974).

[15] Dowling, J., [*The Retina: An Approachable Part of the Brain*], Harvard Univ. Press (1987).

[16] Alexander, K. R., Barnes, C. S., Fishman, G. A., Pokorny, J., and Smith, V. C., "Contrast Sensitivity Deficits in Inferred Magnocellular and Parvocellular Pathways in Retinitis Pigmentosa," *Invest. Ophthalmol. Vis. Sci.* **45**(12), 4510–4519 (2004).

[17] Hahn, L. W. and Geisler, W. S., "Adaptation mechanisms in spatial vision–i. bleaches and backgrounds," *Vision Research* **35**(11), 1585 – 1594 (1995).

[18] Lennie, P., "Roles of M and P pathways," in [*Contrast Sensitivity*], Shapley, R. and Lam, D. M.-K., eds., ch. 11, 201– 213, MIT Press (1993).

[19] Leonova, A., Pokorny, J., and Smith, V. C., "Spatial frequency processing in inferred pc- and mc-pathways," *Vision Research* **43**(20), 2133 – 2139 (2003).

[20] Daly, S., "The visible differences predictor: An algorithm for the assessment of image fidelity," in [*Digital Images and Human Vision*], Watson, A. B., ed., 179– 206, MIT Press (1993).

[21] Mantiuk, R., Daly, S., Myszkowski, K., and Seidel, H.-P., "Predicting visible differences in high dynamic range images – model and its calibration," in [*HVEI X, IS&T/SPIE'05*], **5666**, 204–214 (2005).

[22] Burt, P. J. and Adelson, E. H., "The laplacian pyramid as a compact image code," *IEEE Transactions on Communications* **Com–31**, 532– 540 (1983).

[23] Wilson, H., "A transducer function for threshold and suprathreshold human vision," *Biol. Cybernetics* **38**, 171–178 (1980).

[24] Reinhard, E., Stark, M., Shirley, P., and Ferwerda, J., "Photographic tone reproduction for digital images," in [*SIGGRAPH '02*], 267–276, ACM Press (2002).

[25] Rempel, A. G., Trentacoste, M., Seetzen, H., Young, H. D., Heidrich, W., Whitehead, L., and Ward, G., "Ldr2hdr: on-the-fly reverse tone mapping of legacy video and photographs," in [*SIGGRAPH '07: ACM SIGGRAPH 2007 papers*], 39, ACM, New York, NY, USA (2007).

[26] Akyüz, A. O., Fleming, R., Riecke, B. E., Reinhard, E., and Bülthoff, H. H., "Do HDR Displays Support LDR Content? A Psychophysical Evaluation," *SIGGRAPH'07* **26**(3), 38 (2007).

[27] Čadík, M., Wimmer, M., Neumann, L., and Artusi, A., "Evaluation of HDR tone mapping methods using essential perceptual attributes," *Computers & Graphics* **32**, 330–349 (2008).